

A theoretical study of the interactions of urban breeze circulation with mountain slope winds

Gantuya Ganbat · Jaemyeong Mango Seo ·
Ji-Young Han · Jong-Jin Baik

Received: 19 May 2014 / Accepted: 6 August 2014 / Published online: 21 August 2014
© Springer-Verlag Wien 2014

Abstract A large number of cities around the world are located in or near complex terrain. In these regions, urban breeze circulation and mountain/valley winds are observed. Understanding interactions between urban breeze circulation and mountain/valley winds is important in a view of meso-scale atmospheric dynamics and urban air pollution. In this study, we theoretically examine the interactions of urban breeze circulation with mountain slope winds in the context of the response of the atmosphere to specified thermal forcing. Starting from linearized governing equations in two dimensions, analytical solutions for perturbation vertical velocity, horizontal velocity, buoyancy, and kinematic pressure are obtained. Then, the analytical solutions are used to examine the interactions. Urban breeze circulation and mountain slope winds evolve with time due to time-varying thermal forcing that has steady and diurnal components, and they interact with each other. Asymmetric flows are developed over the urban and mountain areas. In the daytime, low-level converging flows induced by urban heating (urban breeze) and those induced by mountain heating (upslope winds) interfere with each other, resulting in weakened flows in the mountain-side urban area and on the urban-side mountain slope. The transition from the upslope wind to downslope wind on the urban-side mountain slope occurs earlier and thus the downslope wind persists longer compared with the case that has mountain thermal forcing only. In the nighttime, flows become strong in the region between the urban center and the mountain center due to the additive interaction of the downslope wind with the

urban breeze, but the flow intensity weakens with time because of weak nighttime urban heating. In the nighttime, converging flows on the plain-side urban area and the down-slope wind on the rural-side mountain slope are weakened. The degree of the interactions of urban breeze circulation with mountain slope winds is shown to depend on the intensities of urban and mountain thermal forcings.

1 Introduction

Cities around the world have experienced anthropogenic warming with urbanization, featuring higher near-surface air temperature in cities than in surrounding areas, a phenomenon known as the urban heat island. The urban heat island induces local circulation, and this thermally induced local circulation is known as urban breeze circulation. Many observational and numerical modeling studies have been conducted to understand the structure and evolution of urban breeze circulation (e.g., Lemonsu and Masson 2002; Hidalgo et al. 2008a, b; Ryu et al. 2013). These previous studies indicate that urban breeze circulation is deeper, wider, and stronger in the daytime than in the nighttime.

A large number of cities around the world are located in or near complex terrain (e.g., Phoenix, USA; Seoul, South Korea; and Ulaanbaatar, Mongolia). Mountains thermally induce local winds such as mountain/valley winds and up-/down-valley winds. In cities under the influence of mountains, urban breeze circulation interacts with mountain-induced local winds. Some numerical modeling studies have been performed to understand interactions between urban breeze circulation and mountain/valley winds (Savijarvi and Liya 2001; Ohashi and Kida 2002; Lee and Kim 2010; Ryu and Baik 2013). These previous studies indicate that the interactions between

G. Ganbat · J. M. Seo · J.-J. Baik (✉)
School of Earth and Environmental Sciences, Seoul National
University, Seoul 151-742, South Korea
e-mail: jjbaik@snu.ac.kr

J.-Y. Han
Korea Institute of Atmospheric Prediction Systems, Seoul 156-849,
South Korea

urban breeze circulation and mountain/valley winds in the daytime are different from those in the nighttime.

Thermally induced flows/circulation can be theoretically investigated in the context of the response of the atmosphere to specified thermal forcing (see extensive references in Lin 2007). There are a number of linear, theoretical studies that examine urban heat island-induced flows/circulation in the presence of basic-state wind (Olfe and Lee 1971; Lin and Smith 1986; Baik 1992; Han and Baik 2008), demonstrating upward motion downwind of the urban heat island. In these previous studies, the urban heat island is represented by a time-independent surface or low-level heat source. It would be interesting to theoretically examine how urban heat island-induced flows/circulation are/is influenced by mountain/valley winds.

Recently, Ganbat et al. (2014) investigated the two-dimensional interactions of urban breeze circulation with mountain slope winds under no basic-state wind using a mesoscale model that includes an advanced urban canopy model. They demonstrated that daytime circulation over the urban area is characterized by the weakened mountain-side urban wind due to the opposing upslope wind and the strengthened plain-side urban wind. They also demonstrated that as mountain height decreases and urban fraction increases, the transition from the urban-side upslope wind to downslope wind occurs earlier and the urban-side downslope wind persists longer.

This study aims to understand the interactions of urban breeze circulation with mountain slope winds through a linear, theoretical approach, which thus complements the numerical modeling work of Ganbat et al. (2014). Governing equations, solutions, and parameter settings are given in Sect. 2. Theoretical calculation results are presented and discussed in Sect. 3. Summary and conclusions are given in Sect. 4.

2 Governing equations, solutions, and parameter settings

2.1 Governing equations and solutions

Consider a two-dimensional, hydrostatic, nonrotating, Boussinesq airflow system. Equations governing small-amplitude perturbations with constant basic-state horizontal wind and buoyancy frequency in the presence of thermal forcing can be written as

$$\frac{\partial u}{\partial t} + U \frac{\partial u}{\partial x} = -\frac{\partial \pi}{\partial x} - \nu u, \quad (1)$$

$$\frac{\partial \pi}{\partial z} = b, \quad (2)$$

$$\frac{\partial b}{\partial t} + U \frac{\partial b}{\partial x} + N^2 w = \frac{g}{c_p T_0} q - \nu b, \quad (3)$$

$$\frac{\partial u}{\partial x} + \frac{\partial w}{\partial z} = 0. \quad (4)$$

Here, u and w are the perturbation velocities in the x - and z -directions, respectively, π is the perturbation kinematic pressure, b is the perturbation buoyancy, U is the basic-state wind speed in the x -direction, N is the buoyancy frequency, g is the gravitational acceleration, c_p is the specific heat of air at constant pressure, T_0 is the reference temperature, and ν is the coefficient of Rayleigh friction and Newtonian cooling. The thermal forcing q is specified to be bell-shaped in the horizontal, to decrease exponentially with height, and to exhibit diurnal variation:

$$q(x, z, t) = q_0 \frac{a^2}{x^2 + a^2} e^{-z/h} \operatorname{Re}\{e^{i\Omega t}\}, \quad (5)$$

where q_0 is the magnitude of the thermal forcing, a is the half-width of the bell-shaped function, h is the e -folding thermal forcing depth, and Ω is the angular frequency of the diurnal variation.

Combining the above governing equations into a single equation for the perturbation vertical velocity yields

$$\left(\frac{\partial}{\partial t} + U \frac{\partial}{\partial x} + \nu \right)^2 \frac{\partial^2 w}{\partial z^2} + N^2 \frac{\partial^2 w}{\partial x^2} = \frac{g}{c_p T_0} \frac{\partial^2 q}{\partial x^2}. \quad (6)$$

Taking the Fourier transform in x ($\rightarrow k$) and t ($\rightarrow \omega$) upon Eq. (6) obtains

$$\frac{d^2 \hat{w}}{dz^2} + N^2 \lambda^2 \hat{w} = \frac{g}{c_p T_0} \lambda^2 \hat{q}, \quad (7)$$

where

$$\lambda = \frac{k}{(\omega + U k) - i\nu},$$

$$\hat{q}(k, z, \omega) = q_0 a e^{-ak} e^{-z/h} \frac{\delta(\omega - \Omega) + \delta(\omega + \Omega)}{2}.$$

Here, δ is the delta function.

The general solution of Eq. (7) is

$$\hat{w}(k, z, \omega) = A(k, \omega)e^{iN\lambda z} + B(k, \omega)e^{-iN\lambda z} + \frac{\lambda^2 h^2}{1 + N^2 \lambda^2 h^2} \frac{g}{c_p T_0} \hat{q}. \quad (8)$$

Two unknown coefficients $A(k, \omega)$ and $B(k, \omega)$ are determined by imposing a flat bottom boundary condition ($\hat{w} = 0$ at $z=0$) and an upper radiation condition ($B(k, \omega)=0$ for $U \geq 0$). Then, the solution in transformed space becomes

$$\hat{w}(k, z, \omega) = C \frac{\lambda^2}{1 + N^2 \lambda^2 h^2} e^{-ak} \frac{\delta(\omega - \Omega) + \delta(\omega + \Omega)}{2} \left(e^{-z/h} - e^{iN\lambda z} \right), \quad (9)$$

where

$$C = \frac{g}{c_p T_0} q_0 a h^2.$$

The solution for the perturbation vertical velocity in physical space for thermal forcing (Eq. (5)) is obtained by taking the inverse Fourier transform in k ($\rightarrow x$) and ω ($\rightarrow t$) upon Eq. (9):

$$w(x, z, t) = \frac{C}{2} \operatorname{Re} \left\{ \int_0^\infty \left[\frac{\lambda_+^2}{1 + N^2 \lambda_+^2 h^2} \left(e^{-z/h} - e^{iN\lambda_+ z} \right) e^{i\Omega t} + \frac{\lambda_-^2}{1 + N^2 \lambda_-^2 h^2} \left(e^{-z/h} - e^{iN\lambda_- z} \right) e^{-i\Omega t} \right] e^{-ak} e^{ikx} dk \right\}, \quad (10)$$

where

$$\lambda_+ = \frac{k}{(\Omega + U k) - i\nu}, \quad \lambda_- = \frac{k}{(-\Omega + U k) - i\nu}.$$

Taking the real part of Eq. (10) obtains

$$w(x, z, t) = \frac{C}{2} \int_0^\infty k^2 e^{-ak} \left\{ X_R \left[e^{-z/h} \cos(kx + \Omega t) - e^{-\gamma z} \cos(kx + mz + \Omega t) \right] - X_1 \left[e^{-z/h} \sin(kx + \Omega t) - e^{-\gamma z} \sin(kx + mz + \Omega t) \right] + X_R' \left[e^{-z/h} \cos(kx - \Omega t) - e^{-\gamma' z} \cos(kx + m' z - \Omega t) \right] - X_1' \left[e^{-z/h} \sin(kx - \Omega t) - e^{-\gamma' z} \sin(kx + m' z - \Omega t) \right] \right\} dk, \quad (11)$$

where

$$\begin{aligned} X_R &= \frac{(\Omega + U k)^2 + N^2 h^2 k^2 - \nu^2}{\left[(\Omega + U k)^2 + N^2 h^2 k^2 - \nu^2 \right]^2 + 4\nu^2 (\Omega + U k)^2}, \\ X_1 &= \frac{2\nu(\Omega + U k)}{\left[(\Omega + U k)^2 + N^2 h^2 k^2 - \nu^2 \right]^2 + 4\nu^2 (\Omega + U k)^2}, \\ X_R' &= \frac{(\Omega - U k)^2 + N^2 h^2 k^2 - \nu^2}{\left[(\Omega - U k)^2 + N^2 h^2 k^2 - \nu^2 \right]^2 + 4\nu^2 (\Omega - U k)^2}, \\ X_1' &= \frac{-2\nu(\Omega - U k)}{\left[(\Omega - U k)^2 + N^2 h^2 k^2 - \nu^2 \right]^2 + 4\nu^2 (\Omega - U k)^2}, \\ \gamma &= \frac{N k \nu}{(\Omega + U k)^2 + \nu^2}, \quad m = \frac{N k (\Omega + U k)}{(\Omega + U k)^2 + \nu^2}, \\ \gamma' &= \frac{N k \nu}{(\Omega - U k)^2 + \nu^2}, \quad m' = \frac{-N k (\Omega - U k)}{(\Omega - U k)^2 + \nu^2}. \end{aligned}$$

The solutions for the perturbation horizontal velocity, perturbation buoyancy, and perturbation kinematic pressure can be obtained using Eq. (11) and the transformed equations of (1)–(4). These are, respectively, given by

$$\begin{aligned} u(x, z, t) &= \frac{C}{2} \int_0^\infty k e^{-ak} \left\{ X_R \left[h^{-1} e^{-z/h} \sin(kx + \Omega t) + e^{-\gamma z} \{ m \cos(kx + mz + \Omega t) - \gamma \sin(kx + mz + \Omega t) \} \right] \right. \\ &\quad + X_1 \left[h^{-1} e^{-z/h} \cos(kx + \Omega t) - e^{-\gamma z} \{ m \sin(kx + mz + \Omega t) + \gamma \cos(kx + mz + \Omega t) \} \right] \\ &\quad + X_R' \left[h^{-1} e^{-z/h} \sin(kx - \Omega t) + e^{-\gamma' z} \{ m' \cos(kx + m' z - \Omega t) - \gamma' \sin(kx + m' z - \Omega t) \} \right] \\ &\quad + X_1' \left[h^{-1} e^{-z/h} \cos(kx - \Omega t) - e^{-\gamma' z} \{ m' \sin(kx + m' z - \Omega t) + \gamma' \cos(kx + m' z - \Omega t) \} \right] \left. \right\} dk, \end{aligned} \quad (12)$$

$$\begin{aligned} b(x, z, t) &= -\frac{C}{2} \int_0^\infty k e^{-ak} \left\{ Y_R \left[h^{-2} e^{-z/h} \cos(kx + \Omega t) + e^{-\gamma z} \{ (m^2 - \gamma^2) \cos(kx + mz + \Omega t) - 2m\gamma \sin(kx + mz + \Omega t) \} \right] \right. \\ &\quad - Y_1 \left[h^{-2} e^{-z/h} \sin(kx + \Omega t) + e^{-\gamma z} \{ (m^2 - \gamma^2) \sin(kx + mz + \Omega t) + 2m\gamma \cos(kx + mz + \Omega t) \} \right] \\ &\quad + Y_R' \left[h^{-2} e^{-z/h} \cos(kx - \Omega t) + e^{-\gamma' z} \{ (m'^2 - \gamma'^2) \cos(kx + m' z - \Omega t) - 2m'\gamma' \sin(kx + m' z - \Omega t) \} \right] \\ &\quad - Y_1' \left[h^{-2} e^{-z/h} \sin(kx - \Omega t) + e^{-\gamma' z} \{ (m'^2 - \gamma'^2) \sin(kx + m' z - \Omega t) + 2m'\gamma' \cos(kx + m' z - \Omega t) \} \right] \left. \right\} dk, \end{aligned} \quad (13)$$

$$\begin{aligned}
\pi(x, z, t) = & \frac{C}{2} \int_0^\infty k e^{-ak} \left\{ Y_R \left[h^{-1} e^{-z/h} \cos(kx + \Omega t) \right. \right. \\
& - e^{-\gamma z} \{ m \sin(kx + mz + \Omega t) + \gamma \cos(kx + mz + \Omega t) \} \} \\
& - Y_I \left[h^{-1} e^{-z/h} \sin(kx + \Omega t) \right. \\
& + e^{-\gamma z} \{ m \cos(kx + mz + \Omega t) - \gamma \sin(kx + mz + \Omega t) \} \} \\
& + Y_R' \left[h^{-1} e^{-z/h} \cos(kx - \Omega t) \right. \\
& + e^{-\gamma' z} \left\{ m' \sin(kx + m'z - \Omega t) - \gamma' \cos(kx + m'z - \Omega t) \right\} \} \\
& + Y_I' \left[h^{-1} e^{-z/h} \sin(kx - \Omega t) \right. \\
& - e^{-\gamma' z} \left\{ m' \cos(kx + m'z - \Omega t) + \gamma' \sin(kx + m'z - \Omega t) \right\} \} \} dk, \\
(14)
\end{aligned}$$

where

$$Y_R = Y_R' = \nu X_R - \Omega X_I, \quad Y_I = -Y_I' = \Omega X_R + \nu X_I.$$

The integrations with respect to k in Eqs. (11)–(14) are evaluated numerically using the forward scheme.

2.2 Parameter settings

The specified forcing (Eq. (5)) produces thermally induced circulation/flow, and the linear interactions of urban breeze circulation with mountain slope winds can be examined by analyzing the solution obtained by the superposition of a solution for the case of urban breeze circulation and a solution for the case of mountain slope winds. Solutions for individual cases are the same (given by Eqs. (11)–(14)) but with some different parameter values suitable for individual cases. The thermal forcing that induces urban breeze circulation (mountain slope winds) is supposed to have a steady component and a diurnally varying component. Then, the solution for the perturbation vertical velocity is expressed by

$$\begin{aligned}
w(x, z, t) = & w_{us}(x - c_u, z, t - \tau_u) + w_{ud}(x - c_u, z, t - \tau_u) \\
& + w_{ms}(x - c_m, z, t - \tau_m) + w_{md}(x - c_m, z, t - \tau_m).
\end{aligned}
(15)$$

Here, w_{us} and w_{ud} are the perturbation vertical velocities corresponding to a steady thermal forcing component and a diurnally varying thermal forcing component, respectively, for the case of urban breeze circulation. The magnitudes of steady and diurnally varying thermal forcings for the case of urban breeze circulation are denoted by q_{us} and q_{ud} , respectively. w_{ms} and w_{md} are the perturbation vertical velocities corresponding to steady and diurnally varying thermal forcing components, respectively, for the case of mountain slope winds. The magnitudes of steady and diurnally varying thermal forcings for the case of mountain slope winds are denoted

by q_{ms} and q_{md} , respectively. c_u (c_m) is the center of thermal forcing for the case of urban breeze circulation (mountain slope winds), and τ_u (τ_m) is the time of the maximum thermal forcing for the case of urban breeze circulation (mountain slope winds).

An urban area (mountain area) is mainly located from $x=0$ to 20 km (from $x=-20$ to 0 km). The parameter values are specified as $c_u=10$ km, $c_m=-10$ km, $\tau_u=1700$ LT, $\tau_m=1400$ LT, $a_u=a_m=5$ km (half-width of thermal forcing, subscript u (m) denoting the urban (mountain)), $N=0.01$ s⁻¹, and $T_0=283$ K. The values of τ_u and τ_m are chosen based upon the results of Ganbat et al. (2014). Note that the angular frequency of the steady thermal forcing component is 0 s⁻¹ and that of the diurnally varying thermal forcing component is $2\pi/24$ h⁻¹.

Figure 1 shows the temporal variations of urban thermal forcing at $x=c_u$ and $z=0$ km and mountain thermal forcing at $x=c_m$ and $z=0$ km. Here, $q_{us}=0.20$, $q_{ud}=0.15$, $q_{ms}=0.05$, and $q_{md}=0.20$ J kg⁻¹ s⁻¹ are used. Urban breeze circulation is induced by the temporally varying positive thermal forcing (heating) in the urban area. Mountain slope winds are induced by the temporally varying positive/negative thermal forcing (heating/cooling) in the mountain area. Although not included in the present theoretical study, the topographical structure can also affect mountain slope winds. Recently, Kirshbaum (2013) compared the circulation induced by horizontally varying surface heating over Gaussian terrain with the circulation induced by localized heating over flat terrain. The analysis results indicate that the circulation induced by heating over flat terrain can reproduce the circulation induced by surface heating over Gaussian terrain. The finding of Kirshbaum (2013) provides a justification for imposing heating/cooling only in the present study, although a further study that includes the topographic effect is needed.

This study considers no basic-state wind. Under this condition, ν should be positive to obtain a physical solution to steady thermal forcing component because the γ and γ' in

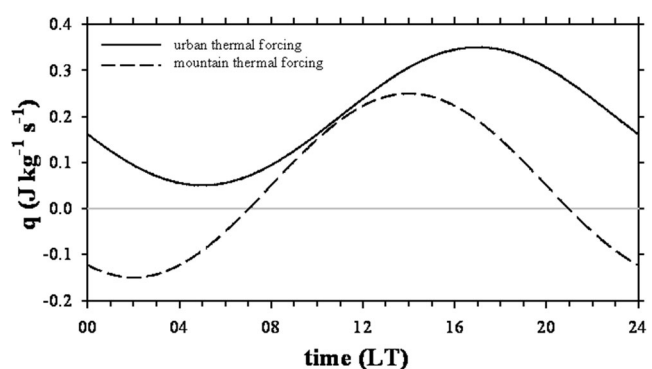


Fig. 1 Temporal variations of urban thermal forcing at $x=c_u$ and $z=0$ km (solid line) and mountain thermal forcing at $x=c_m$ and $z=0$ km (dashed line)

exponents in Eq. (11) become infinite in an inviscid system. In this study, $\nu=1/7,200 \text{ s}^{-1}$ is chosen. The e -folding depth of thermal forcing is determined to have a height of maximum vertical velocity similar to that of Ganbat et al. (2014): $h=750 \text{ m}$ for the case of urban breeze circulation and $h=500 \text{ m}$ for the case of mountain slope winds. Seven cases with different thermal forcing magnitudes are examined in Sect. 3.1 and Sect. 3.2. Table 1 lists the names and thermal forcing magnitudes for individual cases. Hereafter, for brevity, the perturbation vertical velocity, perturbation horizontal velocity, perturbation velocity vector, perturbation buoyancy, and perturbation kinematic pressure are designated as the vertical velocity, horizontal velocity, velocity vector, buoyancy, and kinematic pressure, respectively.

3 Results and discussion

3.1 Urban breeze circulation and mountain slope winds

Figure 2a–e shows the kinematic pressure, buoyancy, vertical velocity, and velocity vector fields at 0200, 0800, 1400, 1700, and 2000 LT in the urban case with $q_{us}=0.20$, $q_{ud}=0.15$, $q_{ms}=0$, and $q_{md}=0 \text{ J kg}^{-1} \text{ s}^{-1}$. At 0200 LT, the low pressure and the weak positive buoyancy centered at $x=10 \text{ km}$ and $z=0 \text{ km}$ drive low-level converging flows toward the urban center and relatively strong upward motion there. Weak upper-level diverging flows and weak downward motion appear outside the urban area. At 0800 LT, the urban breeze circulation is very weak. The urban breeze circulation intensifies and the layer of low-level converging flows becomes thick as the urban heating increases (Fig. 2c, d). At 1700 LT, the horizontal size of the urban breeze circulation is 2.9 times the urban size and its vertical size is 2.2 km. Here, the horizontal (vertical) size of the urban breeze circulation is determined as the horizontal (vertical) extent where the surface horizontal velocity (the vertical

velocity) is larger than 0.2 (0.1) times its maximum value. At 2000 LT, the urban breeze circulation is still strong.

Figure 2f–j shows the kinematic pressure, buoyancy, vertical velocity, and velocity vector fields at 0200, 0800, 1400, 1700, and 2000 LT in the mount case with $q_{us}=0$, $q_{ud}=0$, $q_{ms}=0.05$, and $q_{md}=0.20 \text{ J kg}^{-1} \text{ s}^{-1}$. Note that cooling exists from 2100 to 0700 LT and heating exists from 0700 to 2100 LT (Fig. 1). Unlike the urban breeze circulation, as the mountain thermal forcing changes its sign twice a day, the mountain slope wind also changes its direction twice a day. At 0200 LT, the high pressure and negative buoyancy centered at $x=-10 \text{ km}$ and $z=0 \text{ km}$ drive low-level diverging flows away from the mountain center and relatively strong downward motion there. Upper-level converging flows and weak upward motion appear outside the mountain area. These features are different from those of the urban breeze circulation (Fig. 2a, f). At 0800 LT, the mountain circulation is very weak. At 1400 and 1700 LT, circulation features are similar to those of urban breeze circulation (Fig. 2c, d, h, i). At 2000 LT, the mountain circulation is weak. Physically, the diverging (converging) flows in the mountain area are downslope (upslope) winds. The transition from the upslope wind to downslope wind at a midslope location ($x=-5 \text{ km}$) occurs at 2313 LT. The occurrence frequency of the downslope (upslope) wind at the midslope location is 42 % (58 %) during the 24-h period.

Figure 3 shows the temporal variations of the maximum horizontal velocity in the entire domain (u_{\max}) and w_m in $0 \text{ km} \leq x \leq 20 \text{ km}$ and $-20 \text{ km} \leq x \leq 0 \text{ km}$. Here, w_m is taken as the largest value between the maximum and minimum vertical velocities keeping its sign. Different temporal variations in u_{\max} and w_m in the urban and mount cases are associated with different temporal variations of thermal forcing. A lag exists between the time of the strongest thermal forcing and maximal u_{\max} or w_m (Fig. 3). In both urban and mount cases, the time lag is larger for maximal u_{\max} than for the maximal w_m . In the urban case, the maximal u_{\max} occurs 2 h 2 min later than the strongest heating. In the mount case, there are two maxima in u_{\max} . Both the two maxima in u_{\max} occur 2 h 11 min later than the strongest daytime heating (nighttime cooling). The urban heating induces upward motion in the urban area (Fig. 3b), whereas the mountain heating (cooling) induces upward (downward) motion in the mountain area (Fig. 3c). The weaker buoyancy in the mount case than in the urban case results in smaller w_m . The lag between the time of the strongest heating and the time of maximal w_m is 36 min in the urban case and 43 min in the mount case. The lag between the time of the strongest cooling and the time of minima in w_m in the mount case is 43 min.

Figure 4 shows the distance-time sections of the horizontal velocity at the surface and the vertical velocity at $z=200 \text{ m}$. In each of the urban and mount cases, the horizontal velocity is

Table 1 Names and thermal forcing magnitudes for seven cases (unit: $\text{J kg}^{-1} \text{ s}^{-1}$)

Case	q_{us}	q_{ud}	q_{ms}	q_{md}
urban	0.20	0.15	0	0
mount	0	0	0.05	0.20
urban-mount	0.20	0.15	0.05	0.20
urban+	0.30	0.225	0.05	0.20
urban-	0.10	0.075	0.05	0.20
mount+	0.20	0.15	0.075	0.30
mount-	0.20	0.15	0.025	0.10

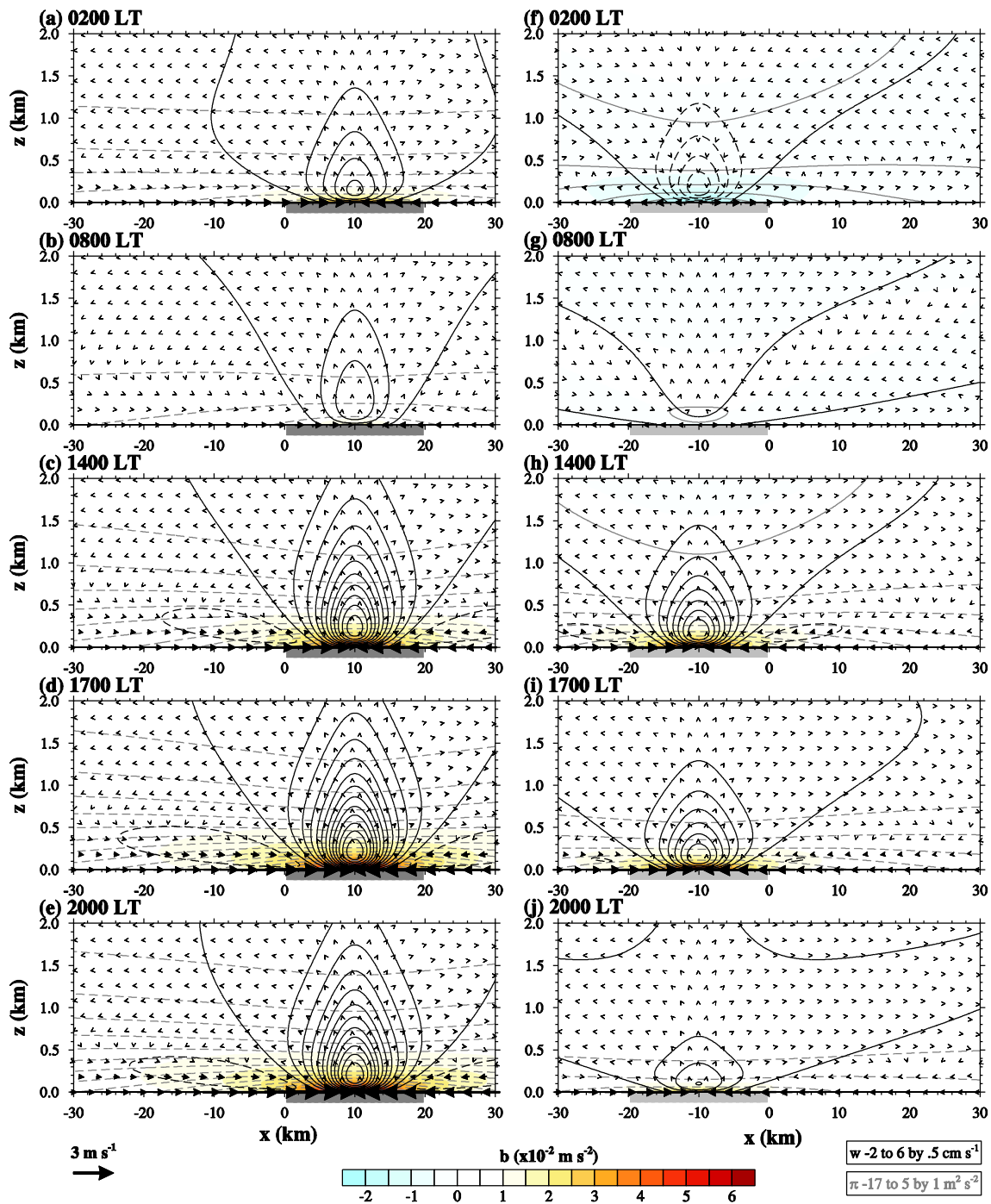


Fig. 2 Kinematic pressure (gray lines), buoyancy (shaded), vertical velocity (black lines), and velocity vector fields at **a, f** 0200, **b, g** 0800, **c, h** 1400, **d, i** 1700, and **e, j** 2000 LT in the urban (left) and mount (right) cases. The dark gray (gray) box on the x -axis (also, in Figs. 4, 5, and 6) indicates the urban (mountain) area

anti-symmetric and the vertical velocity is symmetric about the thermal forcing center. In the urban case, at \sim 0700 LT, the urban breeze circulation is weakest in the horizontal velocity and its horizontal size is smallest (Fig. 4a). The horizontal velocity is strongest at 1902 LT (3.7 m s^{-1}). The vertical velocity is strongest at 1736 LT (6.5 cm s^{-1}). In the mount

case, the magnitude of the mountain heating is larger than that of the mountain cooling, thus producing stronger converging flows/upslope winds in the daytime than diverging flows/downslope winds in the nighttime (Fig. 4b). The maximum (minimum) vertical velocity of 4.0 cm s^{-1} (-2.4) occurs at 1443 LT (0243).

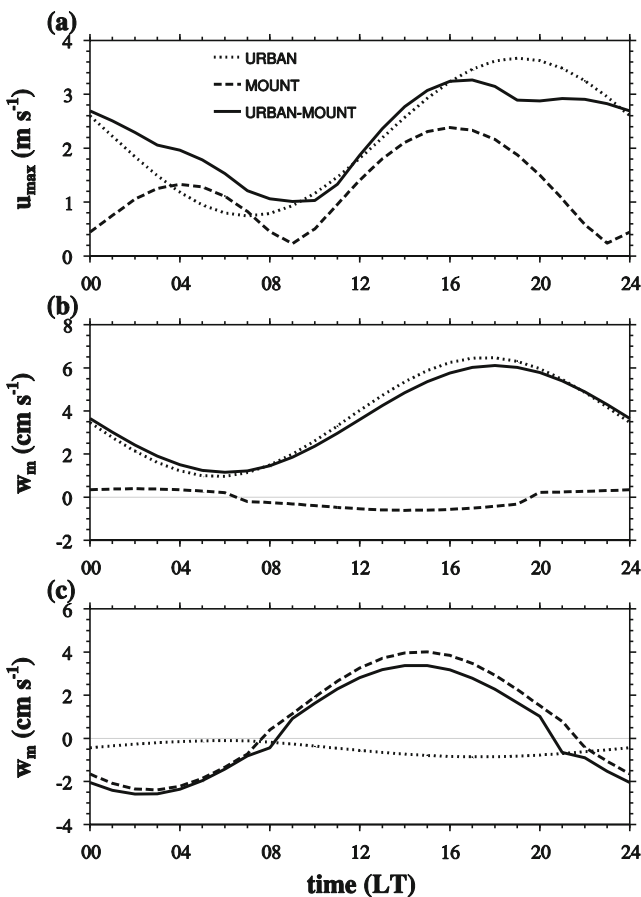


Fig. 3 Temporal variations of **a** the maximum horizontal velocity in the entire domain and w_m in **b** $0 \text{ km} \leq x \leq 20 \text{ km}$ and **c** $-20 \text{ km} \leq x \leq 0 \text{ km}$ in the urban (short-dashed lines), mount (dashed lines), and urban-mount (solid lines) cases

3.2 Interactions of urban breeze circulation with mountain slope winds

For brevity, the following terminologies (Ganbat et al. 2014) are used: mountain-side urban area (from $x=0$ to 10 km), plain-side urban area (from $x=10$ to 20 km), urban-side mountain slope (from $x=-10$ to 0 km), rural-side mountain slope (from $x=-20$ to -10 km), urban-side midslope location ($x=-5$ km), mountain–urban edge ($x=0$ km), and urban–rural edge ($x=20$ km).

Figure 5 shows the kinematic pressure, buoyancy, vertical velocity, and velocity vector fields at 0200, 0800, 1100, 1400, 1700, and 2000 LT in the urban-mount case with $q_{us}=0.20$, $q_{ud}=0.15$, $q_{ms}=0.05$, and $q_{md}=0.20 \text{ J kg}^{-1} \text{ s}^{-1}$. At 0200 LT, positive (negative) buoyancy in the urban (mountain) area is responsible for surface converging (diverging) flows and upward (downward) motion there. The larger pressure gradient between the urban and mountain areas produces stronger winds on the urban-side mountain slope than on the rural-side mountain slope and stronger winds in the mountain-side urban area than in the plain-side urban area. Converging flows

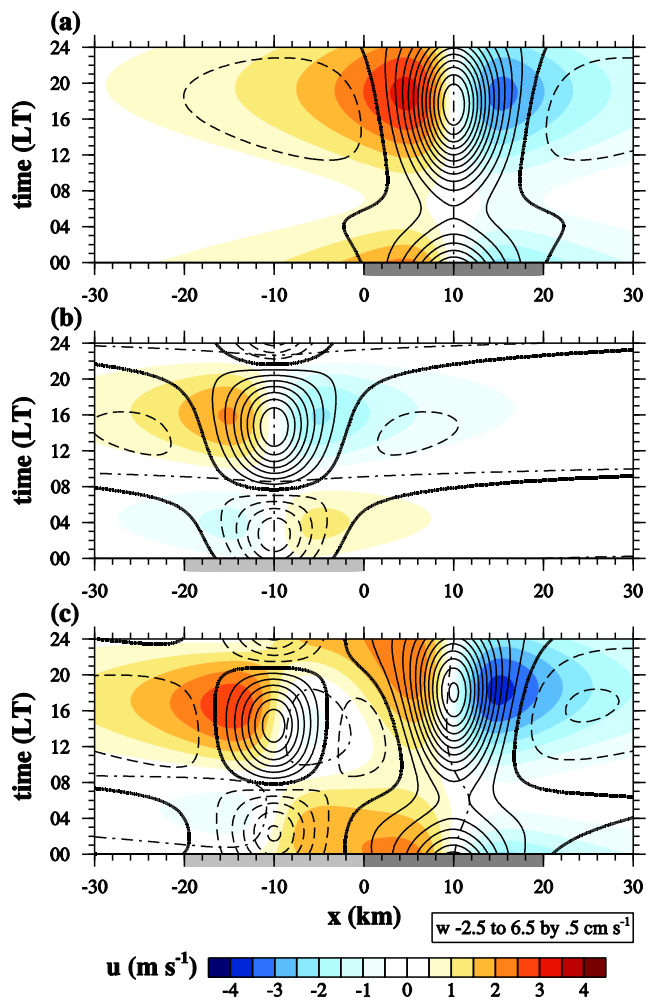


Fig. 4 Distance-time sections of the horizontal velocity (shaded) at the surface and the vertical velocity (solid and dashed lines) at $z=200 \text{ m}$ in the **a** urban, **b** mount, and **c** urban-mount cases. Dashed lines indicate the negative vertical velocity. Bold solid and dashed-short dashed lines indicate the zero vertical and horizontal velocities, respectively

toward the urban center weaken the negative horizontal velocity on the rural-side mountain slope, and diverging flows away from the mountain center weaken the negative horizontal velocity in the plain-side urban area. At 0800 LT, the downslope wind on the urban-side mountain slope is maintained. As the buoyancy in the mountain area becomes positive and strong with time, the converging flows induced by the urban heating and those induced by the mountain heating effectively interfere with each other in the region between $x=-10$ and 10 km, producing weakened upslope winds on the urban-side mountain slope (Fig. 5c). At 1400 and 1700 LT, the upslope wind on the urban-side mountain slope is apparent but weaker than that on the rural-side mountain slope. Moreover, the upslope wind on the urban-side mountain slope is much weaker than the upslope wind in the mount case (Figs. 2h, i and 5d, e). At the urban-side midslope location, the maximum upslope wind is 0.9 m s^{-1} at 1440 LT (2.4 m s^{-1}

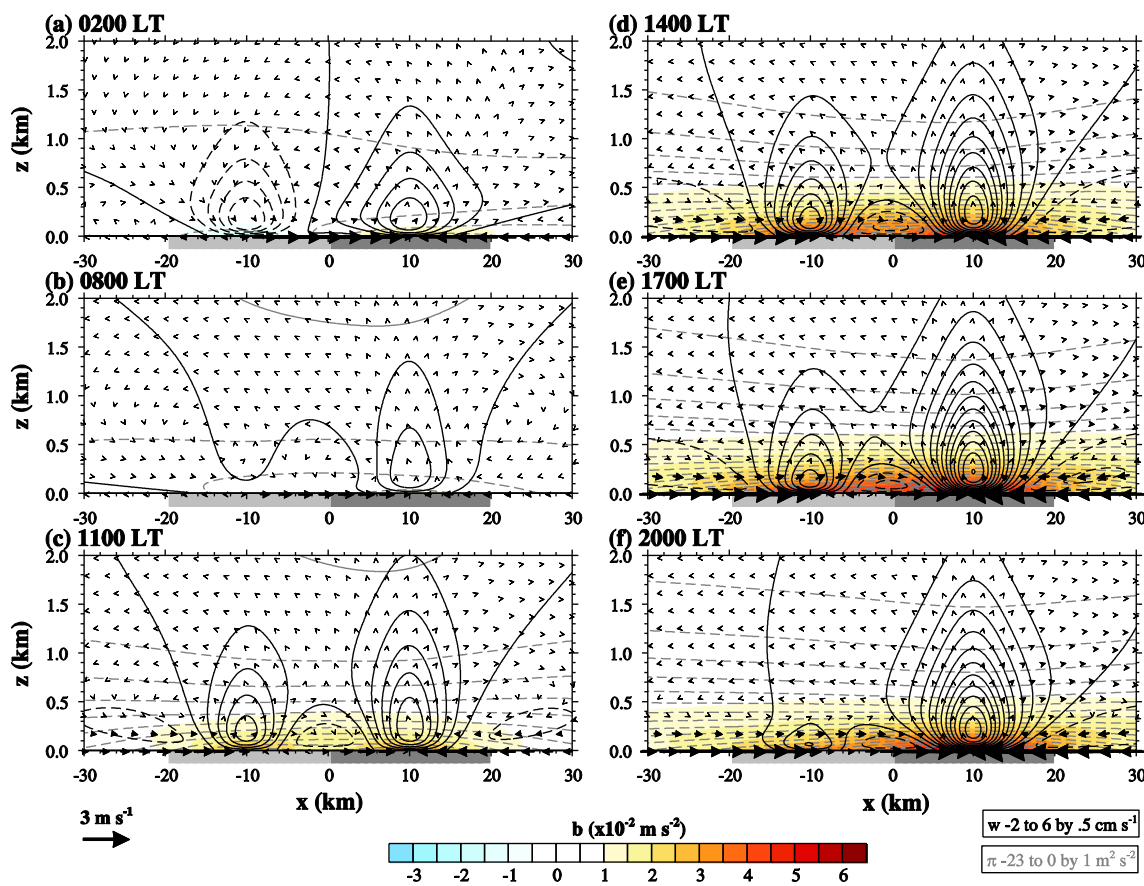


Fig. 5 Kinematic pressure (gray lines), buoyancy (shaded), vertical velocity (black lines), and velocity vector fields at **a** 0200, **b** 0800, **c** 1100, **d** 1400, **e** 1700, and **f** 2000 LT in the urban-mount case

at 1607 LT in the mount case) and the transition from the upslope wind to downslope wind occurs at 1906 LT (4 h 7 min earlier than in the mount case). At 2000 LT, winds on the mountain slope are toward the urban area. At the urban-side midslope location, the occurrence frequency of the downslope (upslope) wind increases (decreases) with its value of 63 % (37 %) in comparison with the mount case due to the interactions of urban breeze circulation with mountain slope winds.

Two features are reflected in the time variation of the maximum horizontal velocity in the urban-mount case (Fig. 3a). From 0300 to 1900 LT, the maximum horizontal velocity displays a time variation similar to that in the urban case. During this period, the maximum horizontal velocity is mostly led by the converging flows induced by the urban heating. From 1900 to 0300 LT, the downslope wind strengthens (weakens) converging flows toward the urban center in the mountain-side (plain-side) urban area. Because of this, the maximum horizontal velocity occurs between the two thermal forcing centers during this period and decreases with time due to the weakening of the urban heating in the nighttime. In the urban area, w_m follows the time variation of the thermal forcing, similar to the urban case (Fig. 3b). Weaker downward (upward) motion beside stronger upward

(downward) motion induced by the mountain thermal forcing in the daytime (nighttime) weakens (strengthens) w_m in the daytime (nighttime) compared with the urban case. Compared with the mount case, in the mountain area, downward motion induced by the urban heating leads to weaker daytime upward motion and stronger nighttime downward motion (Fig. 3c).

In the urban-mount case, flow patterns are not symmetric because of the interactions of urban breezes with mountain slope winds (Fig. 4c). In the nighttime, the downslope wind on the rural-side mountain slope is weakened. Furthermore, the wind in the plain-side urban area reaches its maximum intensity earlier than that in the mountain-side urban area and is weakened due to diverging flows from the mountain. Moreover, converging flows toward the urban area, which is primarily due to the urban heating, intensify the downslope wind on the urban-side mountain slope. Because of this, the downslope wind on the urban-side mountain slope in the urban-mount case starts earlier than that in the mount case. This leads to a longer persistence period of downslope wind. In the daytime, converging flows in the mountain-side urban area are weakened by the upslope wind on the urban-side mountain slope. This is consistent with the results of previous

studies (e.g., Savijarvi and Liya 2001; Ohashi and Kida 2002; Ganbat et al. 2014).

3.3 Sensitivities to thermal forcing intensities

The sensitivities of the interactions between urban breeze circulation and mountain slope winds to urban fraction and maximum mountain height were examined in Ganbat et al. (2014). In this study, analogous sensitivities to different magnitudes of urban and mountain thermal forcings (urban+, urban-, mount+, and mount- cases; Table 1) are examined. In the urban+ (urban-) case, q_{us} and q_{ud} are 1.5 (0.5) times those in the urban-mount case, but q_{ms} and q_{md} are equal to those in the urban-mount case. In the mount+ (mount-) case,

q_{ms} and q_{md} are 1.5 (0.5) times those in the urban-mount case, but q_{us} and q_{ud} are equal to those in the urban-mount case.

Figure 6 shows the kinematic pressure, buoyancy, vertical velocity, and velocity vector fields at 0200 and 1700 LT in the urban+, urban-, mount+, and mount- cases. In the nighttime, the downslope wind is strongly associated with the differences in kinematic pressure and buoyancy between the urban and mountain areas. At 0200 LT, the maximum horizontal velocity is 3.2 m s^{-1} (2.5) at $x=4.9 \text{ km}$ (-4.9 km) in the urban+ (mount+) case and 1.5 m s^{-1} (2.1) at $x=-4.9 \text{ km}$ (5.0) in the urban- (mount-) case (Fig. 6a-d). The strongest wind tends to occur closer to the center of stronger thermal forcing. At 1700 LT, cancellation or enhancement of converging flows is apparent depending on the area (Fig. 6e-h). At 1700 LT, the maximum intensity of upslope wind on the rural-side mountain slope is

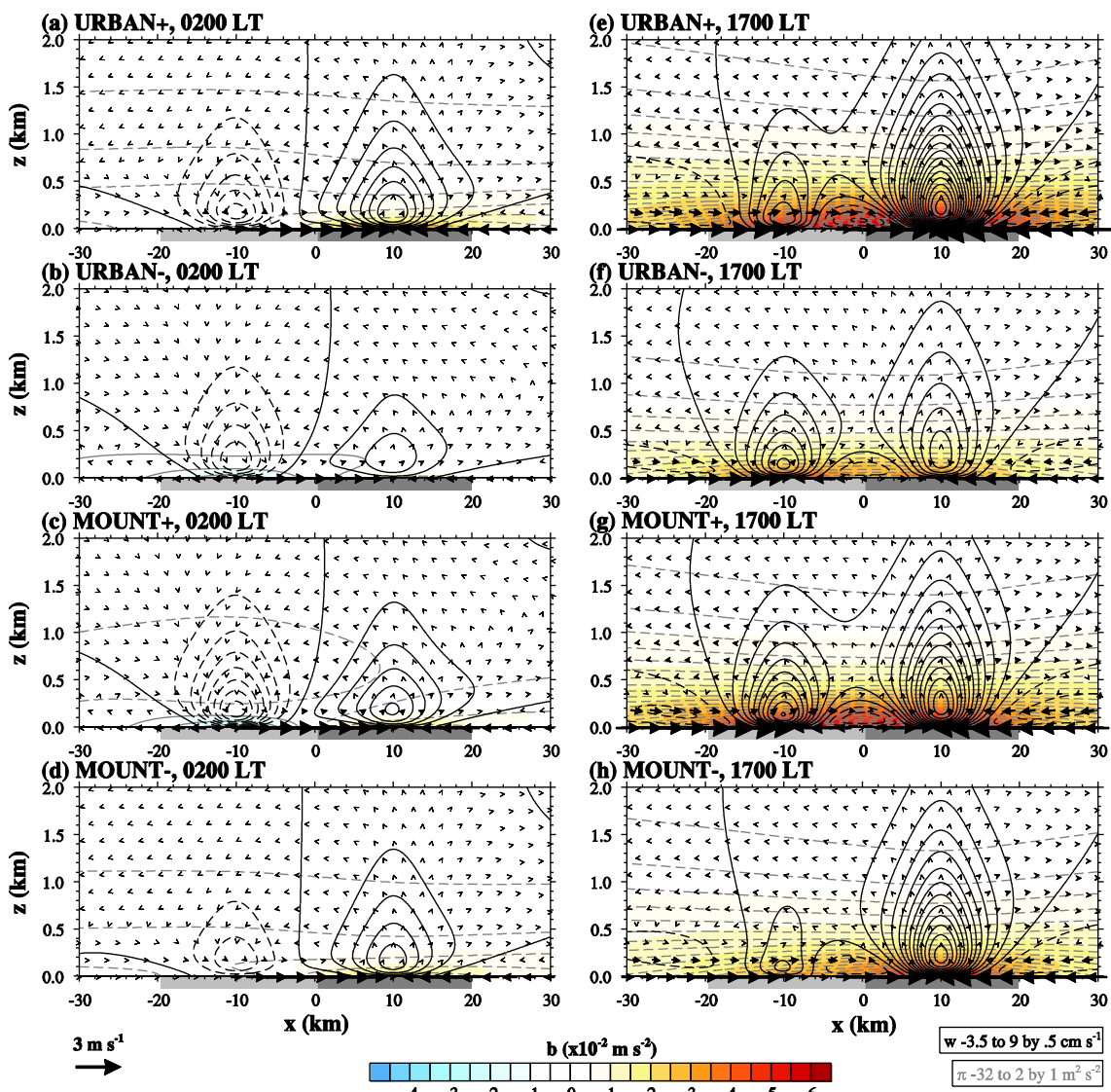


Fig. 6 Kinematic pressure (gray lines), buoyancy (shaded), vertical velocity (black lines), and velocity vector fields at **a–d** 0200 and **e–h** 1700 LT in the urban+ (**a**, **e**), urban- (**b**, **f**), mount+ (**c**, **g**), and mount- (**d**, **h**) cases

3.7 m s^{-1} (2.8) at $x=-14.0 \text{ km}$ (-14.4 km) in the urban+ (urban-) case and the wind in the plain-side urban area is 4.3 m s^{-1} (3.7) at $x=14.4 \text{ km}$ (14.6 km) in the mount+ (mount-) case. This result indicates that the enhancement of the upslope wind on the rural-side mountain slope (wind in the plain-side urban area) is related to the heating magnitude in the urban (mountain) area. A stagnant point, where the horizontal velocity is zero, is present between the two heating centers due to cancellation of the converging flows toward the heating centers. The stagnant point or the location of u_{\min} (the minimum horizontal velocity in the entire domain) is shifted depending on the heating magnitude and is located closer to the center of weaker heating. The stagnant points are located at $x=-2.6, 1.8$, and 0.0 km in the urban-mount, urban-, and mount+ cases, respectively. In the urban+ and mount- cases, the stagnant points do not exist because converging flows toward the urban heating center are much stronger than converging flows toward the mountain heating center due to the strong urban heating magnitude.

The dependencies of the interactions of urban breeze circulation with mountain slope winds on thermal forcing intensities are examined further in the following. Figure 7 shows the maximum intensities of the horizontal velocity at the mountain–urban and urban–rural edges, the transition time from the upslope wind to downslope wind at the urban-side midslope location, and the percentage of the occurrence frequency of downslope wind at the urban-side midslope location as a function of the ratios of thermal forcing magnitudes. Here, R_u (R_m) indicates the ratio of each magnitude of the urban (mountain) thermal forcing in any case to that in the urban-mount case.

The maximum intensity of the horizontal velocity (u_{\max}) at the mountain–urban edge as a function of R_u and R_m is depicted in Fig. 7a. In Fig. 7a, the gray solid line ($R_m=4.35R_u$) indicates zero u_{\max} . u_{\max} has a negative sign in the area of $R_m>4.35R_u$ and a positive sign in the area of $R_m<4.35R_u$. In both areas, u_{\max} increases with R_u for a given R_m . Moreover, the area of $R_m\leq4.35R_u$ can be divided into two areas by the gray dashed curve (Fig. 7a). In the area below the gray dashed curve, u_{\max} decreases with increasing R_m for a given R_u due to intensified upslope winds in the daytime. In the area above the gray dashed curve, u_{\max} increases with increasing R_m for a given R_u . This maximum intensity occurs in the nighttime due to the strong downslope winds induced by cooling in the mountain area. At the urban–rural edge, the sensitivity of u_{\max} to R_u is large for a given R_m , whereas that to R_m for a given R_u is small (Fig. 7b). The maximum intensity of the horizontal velocity linearly increases with R_u and R_m ($u|_{x=20 \text{ km}}=2.7R_u+0.4R_m$).

The transition from the upslope wind to downslope wind at the urban-side midslope location occurs when $R_m>0.58R_u$ (Fig. 7c). For $R_m<0.58R_u$ (dotted area in Fig. 7c), the upslope wind does not exist at the urban-side midslope location during

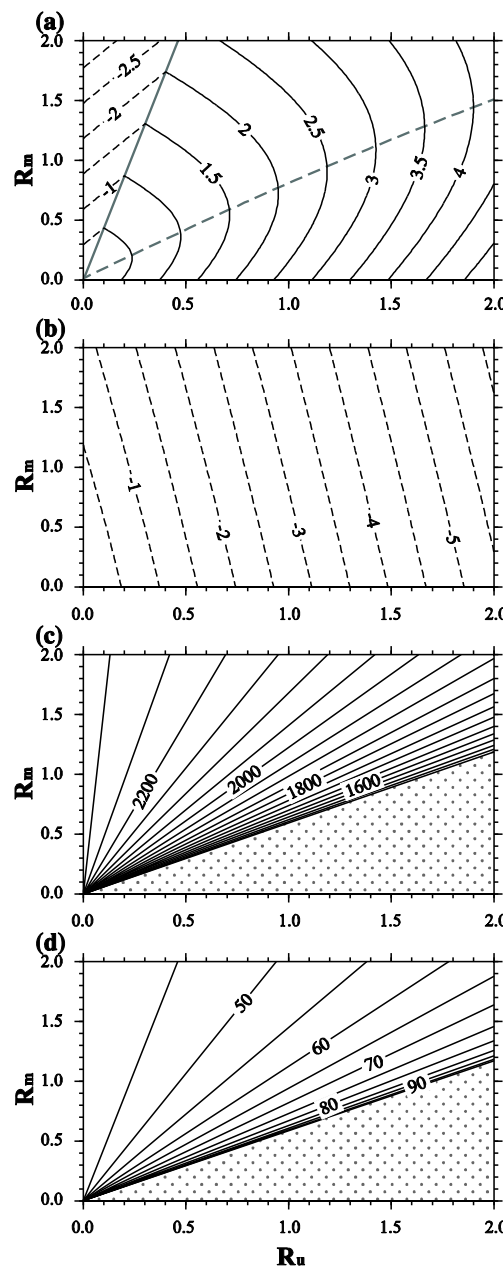


Fig. 7 Maximum intensities of the horizontal velocity (m s^{-1}) at the **a** mountain–urban edge and **b** urban–rural edge, **c** the transition time (LT) from the upslope wind to downslope wind, and **d** the percentage of the occurrence frequency of downslope wind during the 24-h period as a function of the ratios of thermal forcing magnitudes. **c** and **d** are at the urban-side midslope location. The dotted area in **(c)** indicates that the upslope wind does not occur. The dotted area in **(d)** indicates 100 % of the frequency of downslope wind

the 24-h period. The transition from the upslope wind to downslope wind occurs earlier for larger R_u and smaller R_m . For a given R_m (R_u), the transition from the upslope wind to downslope wind starts earlier as R_u increases (R_m decreases). The sensitivity of the occurrence frequency of downslope wind at the urban-side midslope location to R_u and R_m exhibits a pattern similar to that of the transition time from the upslope

wind to downslope wind (Fig. 7d). As the transition from the upslope wind to downslope wind occurs later, the occurrence frequency of downslope wind is small. For $R_m \leq 0.58R_u$ (dotted area in Fig. 7d), only the downslope wind exists at the urban-side midslope location during the 24-h period. The occurrence frequency of downslope wind is large for large R_u and small R_m . For a given R_m (R_u), the occurrence frequency of downslope wind increases with increasing R_u (decreasing R_m).

4 Summary and conclusions

The interactions of urban breeze circulation with mountain slope winds were theoretically investigated in the context of the response of the atmosphere to specified thermal forcing. Linear, theoretical calculations indicated that in the daytime low-level converging flows induced by urban heating (urban breeze) and those induced by mountain heating (upslope winds) interfere with each other in the region between the urban center and the mountain center. Thus, weakened flows appear in the mountain-side urban area and on the urban-side mountain slope. An earlier transition from the upslope wind to downslope wind on the urban-side mountain slope takes place compared with the case of mountain thermal forcing only. Linear, theoretical calculations revealed that in the nighttime strong flows appear in the region between the urban center and the mountain center due to the additive interaction between the downslope wind and the urban breeze. In the nighttime, weakened converging flows appear on the plain-side urban area and weakened downslope wind appears on the rural-side mountain slope. These linear, theoretical results are largely consistent with the numerical modeling results of Ganbat et al. (2014). Sensitivity analyses indicated that the degree of the interactions between urban breeze circulation and mountain slope winds depends on urban and mountain thermal forcing intensities.

In this study, the buoyancy frequency is assumed to be constant. In the real atmosphere, the buoyancy frequency (stability) in the atmospheric boundary layer varies with time, exhibiting stable stratification in the nighttime and less stable or nearly neutral stratification in the daytime under clear skies. The boundary-layer stability can greatly affect thermally induced circulation/flows (Baik et al. 2007). A time-varying buoyancy frequency needs to be taken into account in future studies. In this study, the two-dimensional interactions of urban breeze circulation with mountain slope winds were investigated. In three dimensions, realistic urban geometries and various mountain shapes can be considered, which is thus

expected to produce complex but very interesting thermally induced circulation/flows and interactions. An extension of this study to three dimensions would be worthwhile.

Acknowledgments The authors are grateful to one anonymous reviewer for providing valuable comments on this work. The first, second, and fourth authors were supported by the National Research Foundation of Korea (NRF) grant funded by the Korea Ministry of Science, ICT and Future Planning (MSIP) (No. 2011-0017041). The third author was supported by the R&D project on the development of Korea's global numerical weather prediction systems of Korea Institute of Atmospheric Prediction Systems (KIAPS) funded by the Korea Meteorological Administration (KMA).

References

- Baik JJ (1992) Response of a stably stratified atmosphere to low-level heating—an application to the heat island problem. *J Appl Meteorol* 31:291–303
- Baik JJ, Kim YH, Kim JJ, Han JY (2007) Effects of boundary-layer stability on urban heat island-induced circulation. *Theor Appl Climatol* 89:73–81
- Ganbat G, Baik JJ, Ryu YH (2014) A numerical study of the interactions of urban breeze circulation with mountain slope winds. *Theor Appl Climatol* doi:[10.1007/s00704-014-1162-7](https://doi.org/10.1007/s00704-014-1162-7)
- Han JY, Baik JJ (2008) A theoretical and numerical study of urban heat island-induced circulation and convection. *J Atmos Sci* 65:1859–1877
- Hidalgo J, Masson V, Pigeon G (2008a) Urban-breeze circulation during the CAPITOUL experiment: numerical simulations. *Meteorol Atmos Phys* 102:243–262
- Hidalgo J, Pigeon G, Masson V (2008b) Urban-breeze circulation during the CAPITOUL experiment: observational data analysis approach. *Meteorol Atmos Phys* 102:223–241
- Kirshbaum DJ (2013) On thermally forced circulations over heated terrain. *J Atmos Sci* 70:1690–1709
- Lee SH, Kim HD (2010) Modification of nocturnal drainage flow due to urban surface heat flux. *Asia-Pac J Atmos Sci* 46:453–465
- Lemonsu A, Masson V (2002) Simulation of a summer urban breeze over Paris. *Bound-Layer Meteor* 104:463–490
- Lin YL (2007) Mesoscale dynamics. Cambridge University Press, Cambridge
- Lin YL, Smith RB (1986) Transient dynamics of airflow near a local heat source. *J Atmos Sci* 43:40–49
- Ohashi Y, Kida H (2002) Effects of mountains and urban areas on daytime local-circulations in the Osaka and Kyoto regions. *J Meteorol Soc Japan* 80:539–560
- Olfe DB, Lee RL (1971) Linearized calculations of urban heat island convection effects. *J Atmos Sci* 28:1374–1388
- Ryu YH, Baik JJ (2013) Daytime local circulations and their interactions in the Seoul metropolitan area. *J Appl Meteorol Climatol* 52:784–801
- Ryu YH, Baik JJ, Han JY (2013) Daytime urban breeze circulation and its interaction with convective cells. *Quart J Roy Meteorol Soc* 139: 401–413
- Savijarvi H, Liya J (2001) Local winds in a valley city. *Bound-Layer Meteor* 100:301–319